Qualification of operating conditions to extend oxygen carrier utilization in the scaling up of chemical looping processes

Arturo Cabello, Alberto Abad [*], María T. Izquierdo, P. Gayán, Luis F. de Diego, Francisco García-Labiano, Juan Adánez

Instituto de Carboquímica (ICB-CSIC), Miguel Luesma Castán 4, 50018 Zaragoza, Spain

ABSTRACT

Chemical looping combustion (CLC) is a technology allowing CO_2 capture at low cost. The development of durable oxygen carrier materials is a key factor for the scale-up of CLC. Once a promising oxygen carrier has been identified dedicated studies into the effects of reaction conditions on the durability of these kinds of materials are required in order to improve their reliability before use at industrial scale. This method requires several long-term tests in CLC units each one of them to fixed conditions, which is time consuming and expensive. In this work, a low-effort method using thermogravimetric analysis was developed and validated against a high-effort method requiring the use of an oxygen carrier material for hundreds of hours in a CLC unit. The reaction pathways and variation in physico-chemical properties of a material with 14 wt% CuO impregnated on γ-Al_2O_3 during the course of 300 redox cycles were evaluated as a function of reaction temperature, variation in oxygen carrier conversion (ΔX_s) and degree of oxidation/reduction in every redox cycle. As a result, preferred conditions to be used in a CLC unit were identified. In general, reactivity and mechanical integrity were not affected when the reaction temperature was 800 °C. However, a temperature of 900 °C was found to be potentially suitable when the material was highly reduced in each redox cycle and ΔX_s was low. The use of this method for promising oxygen carriers can boost the identification of long lasting materials for the scale-up of chemical looping processes.

1. Introduction

There is wide recognition of the potential of CO_2 capture and sequestration (CCS) to meet climate change targets [1]. Chemical looping combustion (CLC) allows fuel combustion with intrinsic CO_2 separation from nitrogen in air, resulting in a low energy penalty and reduced CO_2 capture costs [2]. CLC involves the use of an oxygen carrier, usually a metal oxide, to supply the oxygen for fuel combustion. The spent oxygen carrier is then regenerated through oxidation in air, enabling it to be reused for fuel combustion. The CLC process is usually performed in two interconnected fluidized bed reactors: a Fuel reactor (FR) for fuel combustion and an Air reactor (AR) for oxygen carrier regeneration. The oxygen carrier circulates continuously between the two reactors. The CLC process can be adapted to the characteristics of different fuels and is suitable for gaseous (natural gas, syngas, biogas), solid (coal, biomass) and liquid (bio-ethanol, pyrolysis oil) fuels [3].

The oxygen carrier must allow a high conversion of the fuel, and preferably complete conversion. Thus, experience in CLC units was crucial in order to identify suitable operating conditions that would allow the desired high fuel conversion. Most of the works carried out in CLC units have been focused on the determination of suitable operating conditions for it. For example, for gaseous fuels, the minimum values of both reacting temperature and solids circulation rate to achieve complete fuel conversion are determined for a particular oxygen carrier [4]. Moreover, the CO_2 capture may be affected by these conditions in the case of solid fuels [5].

In addition, physical and chemical stability of the oxygen carrier material is a requisite for the successful scale-up of the CLC process. Oxygen carrier particles undergo a high number of redox cycles at high temperature in a CLC unit, which may induce degradation of their physico-chemical properties. Particle integrity can be affected by thermo-chemical stresses [6] and ionic diffusion mechanisms [7]. These effects may be magnified after hundreds of redox cycles, increasing the material loss in fines produced by abrasion and collisions [8]. The chemical stress increases with the variation of the solids conversion,

Nomenclature

d	stoichiometric coefficient for the fuel combustion reaction (2 in the case of burning CH_4), (mol O_2/mol CH_4)
F_{fuel}	molar flow rate of fuel fed to the fuel reactor (mol/s)
m	instantaneous mass of oxygen carrier (kg)
M_{O_2}	molecular weight of gaseous oxygen (kg/mol)
$\dot{m}_{OC}$	solids circulation flowrate (kg/s)
m_{ox}	mass of the oxidized form of the oxygen carrier (kg)
R_{OC}	oxygen transport capacity of the oxygen carrier (kg O / kg oxygen carrier)
T_{AR}	temperature in the air reactor (°C)
T_{FR}	temperature in the fuel reactor (°C)
X_{ox}	oxidation degree or solids conversion for the oxidation reaction (-)
$X_{ox,inAR}$	oxidation degree or conversion of solids at the inlet of the air reactor (-)
$X_{ox,inFR}$	oxidation degree or conversion of solids at the inlet of the fuel reactor (-)

$X_{ox,outFR}$	oxidation degree or conversion of solids at the outlet of the fuel reactor (-)
X_{ox}^{max}	maximum value of the solids conversion for the oxidation reaction (-)
X_{ox}^{min}	minimum value of the solids conversion for the oxidation reaction (-)
$X_{ox}^{0,ox}$	oxidation degree or conversion of solids at the beginning of the oxidation period (-)
$X_{ox}^{0,red}$	oxidation degree or conversion of solids at the beginning of the reduction period (-)
X_{red}	solids conversion for the reduction reaction (-)
Greek symbols	
ΔX_s	variation of solids conversion (-)
$\Delta X_{s,max}$	maximum value of variation of solids conversion (-)
$\Delta X_{s,min}$	minimum value of variation of solids conversion (-)
ϕ	oxygen carrier-to-fuel ratio (-)
η_{comb}	combustion efficiency (-)

ΔX_s, which can promote the deterioration of the material [9]. In a CLC unit, the variation of the solids conversion is affected directly by the existing solids circulation rate, $\dot{m}_{OC}$, which is often characterised by the oxygen carrier to fuel ratio, ϕ, following the relation:

$$\phi = \dot{m}_{OC} \frac{R_{OC}}{dF_{fuel}M_{O_2}} = \frac{\eta_{comb}}{\Delta X_s} \qquad (1)$$

The ϕ parameter is a measure of the oxygen present in the recirculated oxygen carrier potentially available for fuel combustion in relation to the oxygen required by fuel combustion. High solids circulation rates (or high ϕ values) are related to low ΔX_s, i.e. low chemical stress, and vice versa.

Attempts have been made to theoretically predict degradation mechanisms and the lifetime of oxygen carrier particles [10]. However, determining the effect of thermo-chemical stresses on the lifetime of oxygen carrier particles is often a huge task that involves the interpretation and extrapolation of experimental results obtained during long-term combustion tests in CLC units. Operation in a CLC unit presents a number of limitations and challenges that hinder the scale-up of oxygen carrier materials, which need to be addressed by researchers:

- First, it is necessary to have a CLC unit consisting of two interconnected fluidized beds and the required quantity of solids for its operation. Although this point is obvious, it does limit the number of researchers with the capability to evaluate oxygen carrier ageing under CLC conditions [11].
- Operating conditions in the CLC unit should be maintained as constant as possible during the experimental campaign to obtain reliable results and conclusions. Thermo-chemical stress is affected by reaction temperature and variation in solids conversion, ΔX_s, which can affect particle ageing. This point is often disregarded as there are only few works in which operating conditions are kept relatively constant, which may affect the evaluation of particle lifetime.
- Operating time should be high enough to allow hundreds of redox cycles to be performed. However, the time required in which to achieve reliable results is difficult to determine beforehand. For example, the extrapolated lifetime of a Cu-based material after 39 h of operation with the FR at 800 °C and the AR at 950 °C would be 5000 h; however, particles were quickly converted in dust only 3 h later, meaning that the estimated lifetime was reduced to <200 h [12]. According the method introduced by Cabello et al. [13], the attrition rate both in the CLC unit and relative to the standard air jet

index (AJI in ASTM-D-5757), as well as the crushing strength of particles, should be maintained constant during the operating time in order to consider the results reliable.
- A limited number of conditions can be tested in the trials; therefore, experimental conditions should be carefully selected and maintained constant during the experimental period, but the most suitable operation conditions are difficult to determine prior to the experimental campaign. Then, the selection of operation conditions is done by applying the trial and error method during long-term testing in a CLC unit, with the subsequent effort and costs.

Despite the difficulties described, it has been confirmed that the solids circulation rate may affect the durability of the oxygen carrier material, e.g. for materials based on CuMn mixed oxides [14], Mn-ores [15] or CaMn-based perovskites [9], as well as reacting temperature for Cu-based materials [16]. However, suitable operating conditions have been usually chosen by considering only high fuel conversion.

In this respect, Cu-based materials developed by ICB-CSIC and prepared by impregnation on alumina [17] have been extensively characterized in several CLC units. A complete description of the operating conditions and results achieved can be found in Table S1, Supplementary material (SM). Two similar materials have been developed that share preparation method but are differentiated by the alumina used as a support [18], namely Cu14Al_ICB and Cu14Al_Commercial. About 15% of the total operational experience in CLC burning gaseous fuels (5500 h with methane or natural gas [19]) has involved these kinds of Cu-based oxygen carriers. The durability of this material is highly dependent on the operating conditions in the CLC unit, which is evaluated by the AJI value for used particles in Fig. 1. Temperature in the fuel and air reactors has been kept constant during tests and it shows a high relevance on the durability of the particles. Thus, the attrition rate increases with the temperature in the reactors. The variation of the solids conversion has varied between a minimum and a maximum value during each experimental campaign, indicated by $\Delta X_{s,min}$ and $\Delta X_{s,max}$ in Fig. 1. Nevertheless, it can be differentiated tests with high ΔX_s (>0.5) and low ΔX_s (<0.2). Comparing results for used particles at the same temperature, the AJI value is lower as ΔX_s decreases, i.e. as the chemical stress decreases.

To achieve these results a high number of hours of operation in the CLC unit (at least 60 h for each test) was required. In addition, all tests were performed promoting the complete oxidation of the material in the air reactor, i.e. the oxidation conversion at the fuel reactor inlet was $X_{ox,in,FR} = 1$. There are no results about the performance of the material
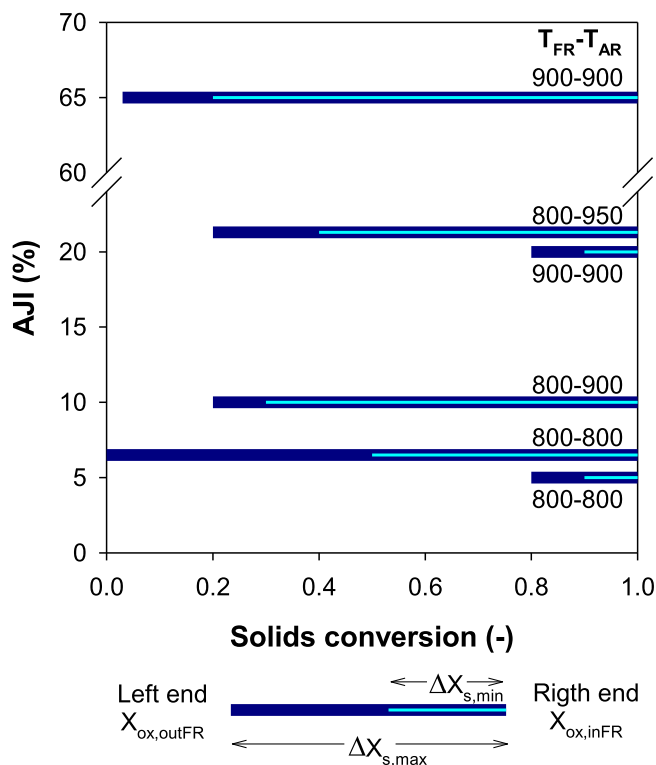
Fig. 1. Attrition (AJI) for particles used in a CLC unit as a function of the variation of the solids conversion in the reactors at different operating temperature in the fuel (T_{FR}) and air (T_{AR}) reactor [16].

considering a partial oxidation of the oxygen carrier in the air reactor. This condition would be possible by decreasing the air excess or adjusting the residence time of solids in the air reactor [20], which would require a high experimental effort again. Therefore, it would be highly recommended to have a reliable tool or method that serves to choose the operating conditions that should be used in a CLC unit. This would be helpful for the development of any material in the future.

A number of attempts have been made -and it continues to be done in the present- to evaluate the ageing of oxygen carrier materials in simpler installations, such as a Thermogravimetric analyser (TGA) [7,21] or batch fluidized bed reactors [17,22]. These studies were based on performing hundreds of redox cycles, and were typically performed only at one temperature and under conditions where the oxygen carrier is highly oxidized during the oxidation period ($X_{ox,in,FR} \approx 1$) and with high chemical stress, i.e. $\Delta X_s \approx 1$, which are not ideal conditions for use in a CLC unit. Therefore, the operating conditions under which long-term trials should be conducted in a CLC unit cannot be deduced from these works.

The aim of this work is to boost oxygen carrier development and the scale-up of the CLC process. A simple method based on performing hundreds of redox cycles under a controlled environment in TGA and the comprehensive characterization of the reacted material was developed and validated against results in CLC units. The novelty of this work includes the study of the effects of reaction temperature, variation in solids conversion and degree of oxidation after regeneration on the physico-chemical stability of a well-known Cu-based oxygen carrier impregnated on γ -Al$_2$O$_3$ during hundreds of redox cycles.

The method presents the following characteristics: the effects of thermo-chemical stress on oxygen carrier particles can be understood; it can be implemented by most researchers involved with gas–solid reaction systems; a small amount of solids is required; and suitable operation conditions in a CLC unit may be deduced from the results achieved. Thus, eventual experimentation in a CLC unit can be guided by the present method with a consequent lessening of the effort required.

2. Experimental

2.1. Oxygen carrier

Cu-based oxygen carrier particles were prepared by the incipient wetness impregnation method [17]. Commercial γ -Al$_2$O$_3$ (Puralox NWa-155, Sasol, Germany GmbH) particles of 0.3–0.5 mm were used as a support. Copper was impregnated at room temperature by adding a volume of copper nitrate solution (5.4 M) to the alumina corresponding to the total pore volume of the support particles (55.4% porosity). The material was then calcined in an air atmosphere for 1 h at 850 °C. The CuO load in the produced particles was 14 wt%, and the material was named Cu14Al_ICB. The material was mainly composed of CuAl$_2$O$_4$ and γ -Al$_2$O$_3$, but speciation of chemical compounds may vary with the operating conditions.

2.2. Experimental procedure

The proposed method considers different oxidation states of the oxygen carrier particles. The oxidation degree is defined by solids conversion for the oxidation reaction, X_{ox}, or the reduction reaction, X_{red}:

$$X_{ox} = 1 - \frac{m_{ox} - m}{m_{ox}R_{OC}} \tag{2}$$

$$X_{red} = \frac{m_{ox} - m}{m_{ox}R_{OC}} \tag{3}$$

The oxidation degree is higher in the AR than in FR, the difference being calculated as:

$$\Delta X_s = X_{ox,AR} - X_{ox,FR} \tag{4}$$

The variation in solids conversion, ΔX_s, is related to the oxygen carrier-to-fuel ratio, ϕ, at which a CLC unit is operated through Eq. (1).

Multiple redox cycles were performed in a TGA (CI Electronics Ltd. [23]) in order to evaluate the effect of particle ageing at different values of conversion variation of the oxygen carrier, ΔX_s. The mass of sample for each test was 150 mg, which was sufficient to enable a deep characterization of the oxygen carrier particles to be performed. The total gas flow was 50 L/h (STP). In each test, 300 redox cycles were performed using H$_2$ for oxygen carrier reduction and diluted air for oxygen carrier oxidation. A purge period with N$_2$ was introduced between the reduction and oxidation stages to prevent the occurrence of O$_2$-H$_2$ mixtures inside the TGA reactor. The conversion variation during reduction and/or oxidation was limited to a given value by controlling the concentration of the reacting gas (H$_2$ or O$_2$) and the reacting time. In all cases, the test series was stopped after the oxidation stage. In the tests where the samples were not fully oxidized, the reactor was cooled down with N$_2$ before sample extraction.

Tables 1 and 2 show the ΔX_s values selected for the tests ranked between 0.1 and 0.95. The variation in ΔX_s simulated the different ϕ values in a CLC unit, which is related to chemical stress on the particles. Tests were designed to simulate different degree of oxidation of the particles:

- The tests shown in Table 1 considered the oxygen carrier to be fully oxidized after the oxidation semi-cycle, simulating an over-sized AR compared to FR -i.e. $X_{ox,AR}$ is maximized. The H$_2$ concentration and the reduction time were subsequently set in order to control the degree of reduction during the reduction semi-cycle.
- Inversely, the tests shown in Table 2 simulated an over-sized FR compared to AR, where particles were highly reduced after the reduction semi-cycle -i.e. $X_{ox,FR}$ is minimized-, as described by Abad et al. [20]. The degree of oxidation during the oxidation semi-cycle was then controlled by setting the O$_2$ concentration and the oxidation time.

Table 1

Experimental conditions for redox cycles in the TGA with the highly oxidized Cu14Al_ICB oxygen carrier ($X_{ox}^{0,red}$=1) after the oxidation stage with 10% O_2.

Temperature (°C)	ΔX_s	$X_{ox}^{max}/X_{ox}^{min}$	H_2 (vol %)	Reduction time (s)	Purge 1 time (s)	O_2 (vol %)	Oxidation time (s)	Purge 2 time (s)	Number of cycles	Total time (h)
800	0.10	1 / 0.90	0.5	30	50	10	120	70	300	~24
800	0.25	1 / 0.75	1.3	30	50	10	120	70	300	~24
800	0.45	1 / 0.55	2.5	30	50	10	120	70	300	~24
800	0.65	1 / 0.35	4.2	30	50	10	120	70	300	~24
800	0.90	1 / 0.10	5.0	60	50	10	120	70	300	~27
900	0.15	1 / 0.85	0.5	20	50	10	120	35	300	~21
900	0.90	1 / 0.10	5.0	45	50	10	120	35	300	~22

Table 2

Experimental conditions for redox cycles in the TGA with the highly reduced Cu14Al_ICB oxygen carrier ($X_{ox}^{0,ox}$ = 0) after the reduction stage with 15% H_2.

Temperature (°C)	ΔX_s	$X_{ox}^{min}/X_{ox}^{max}$	O_2 (vol %)	Oxidation time (s)	Purge 1 time (s)	H_2 (vol %)	Reduction time (s)	Purge 2 time (s)	Number of cycles	Total time (h)
800	0.10	0 / 0.10	0.5	6	60	15	120	60	300	~20
800	0.25	0 / 0.25	1.0	45	60	15	120	60	300	~24
800	0.40	0 / 0.40	3.0	40	60	15	120	60	300	~24
800	0.65	0 / 0.65	5.0	45	60	15	120	60	300	~24
800	0.95	0 / 0.95	5.0	80	60	15	120	60	300	~27
900	0.10	0 / 0.10	0.5	6	30	15	120	60	300	~18
900	0.95	0 / 0.95	5.0	80	30	15	120	60	300	~24

Therefore, the most relevant conditions pertaining to the variation in the degree of oxidation of the oxygen carrier in a CLC unit were simulated by this method. Most of the tests were conducted at 800 °C; but selected tests were performed at 900 °C to evaluate the effect of thermal stress on the physico-chemical properties of the particles.

2.3. Characterization of oxygen carrier particles

The particle microstructure was examined by Scanning electron microscopy with energy dispersive X-ray analysis (SEM-EDX) using a Hitachi S-3400 N scanning electron microscope working with backscattered electrons. Particle porosity was measured by Hg intrusion in a Quantachrome PoreMaster 33. Crushing strength was determined using a Shimpo FGN-5X apparatus by measuring the force needed to fracture a particle. The average value of at least 20 measurements was taken. XRD diffractograms were collected by a Bruker D8 Advance X-ray powder diffractometer equipped with an X-ray source with a Cu anode working at 40 kV and 40 mA, and an energy-dispersive one-dimensional detector. The diffraction pattern was obtained over the 2θ range of 10° to 80° with a step of 0.019°. The assignation of crystalline phases was made according to the Joint Committee on Powder Diffraction Standards. DIF-FRAC.EVA software supports a reference pattern database for phase identification. Quantitative XRD analysis of the crystal phases was performed by Rietveld refinement [24] using TOPAS software. The Inorganic Crystal Structure Database (ICSD) was used to obtain crystal structures of the phases under consideration.

3. Results and discussion

Long-term experiments (c.a. 24 h) were conducted in a TGA by alternating oxidizing and reducing atmospheres. Most of redox cycles were performed at a reaction temperature of 800 °C. This temperature was selected owing to the good behaviour shown by the impregnated Cu-based oxygen carrier Cu14Al_ICB at 800 °C during its use in CLC units [16]. The mechanical stability of the Cu14Al_ICB particles was negatively affected when the reaction temperature in CLC units was increased to 900 °C. However, some tests were also performed at 900 °C to evaluate the effects of thermal stress on oxygen carrier stability in the TGA tests.

3.1. Redox cycles with the highly oxidized oxygen carrier

In this series of experiments, oxidation of the oxygen carrier after reduction in H_2 was enhanced as much as possible, regardless of the degree of reduction achieved in each cycle. The complete evolution of solids conversion during the redox cycles at 800 and 900 °C and several ΔX_s values is shown in SM. In order to evaluate possible changes in the reactivity of the material with the redox cycles, the conversion vs time curves for the different ΔX_s values for both reduction and oxidation in the 1st, 10th, 100th and 300th semi-cycles were examined; see Figs. 2 and 3.

At 800 °C (Fig. 2), the slopes of the conversion vs time curves between the first and 300th cycles were unchanged for both reduction and oxidation periods; i.e. they were parallel. This fact indicates that the material presents high redox stability with regard to reactivity when it reacts at 800 °C, regardless of degree of reduction.

In addition, the oxygen carrier was mostly regenerated after the oxidation stage both at low ($\Delta X_s \approx 0.1$) and high ($\Delta X_s \approx 0.9$) values for variation in oxygen carrier conversion. However, complete re-oxidation was hindered at intermediate values of the conversion variation. Thus, at ΔX_s values of 0.25, 0.45 and 0.65, the degree of oxidation decreased with the redox cycles. Nevertheless, the variation in solids conversion was not affected. As a consequence, the oxygen carrier was reduced to a higher degree as the redox cycles progressed.

Certain differences could be observed at 900 °C; see Fig. 3. When the variation in solids conversion was maintained at low values, e.g. $\Delta X_s \approx$ 0.15, a decrease in final conversion with the cycles was observed in both the reduction and oxidation periods. This fact was accompanied by a decrease in the ability to be regenerated with the redox cycles. This behaviour was clearly observed for the initial 200–250 cycles. In subsequent cycles, the conversion degree after every reduction and oxidation was maintained roughly constant, with the decrease in oxidation conversion being of lesser importance; see Figure S2, SM. This result differs completely from the behaviour observed at 800 °C, where degradation during the reduction and oxidation stages was not observed at $\Delta X_s \approx 0.1$, and was barely perceptible at $\Delta X_s \approx 0.25$.

Also at 900 °C, reduction reactivity was slightly improved when the variation in conversion was high, e.g. $\Delta X_s \approx 0.9$. In this case, the oxygen carrier was able to be almost fully regenerated during the entire redox cycles but the oxidation process showed intriguing behaviour: the number of redox cycles did not affect reactivity until approximately 60%
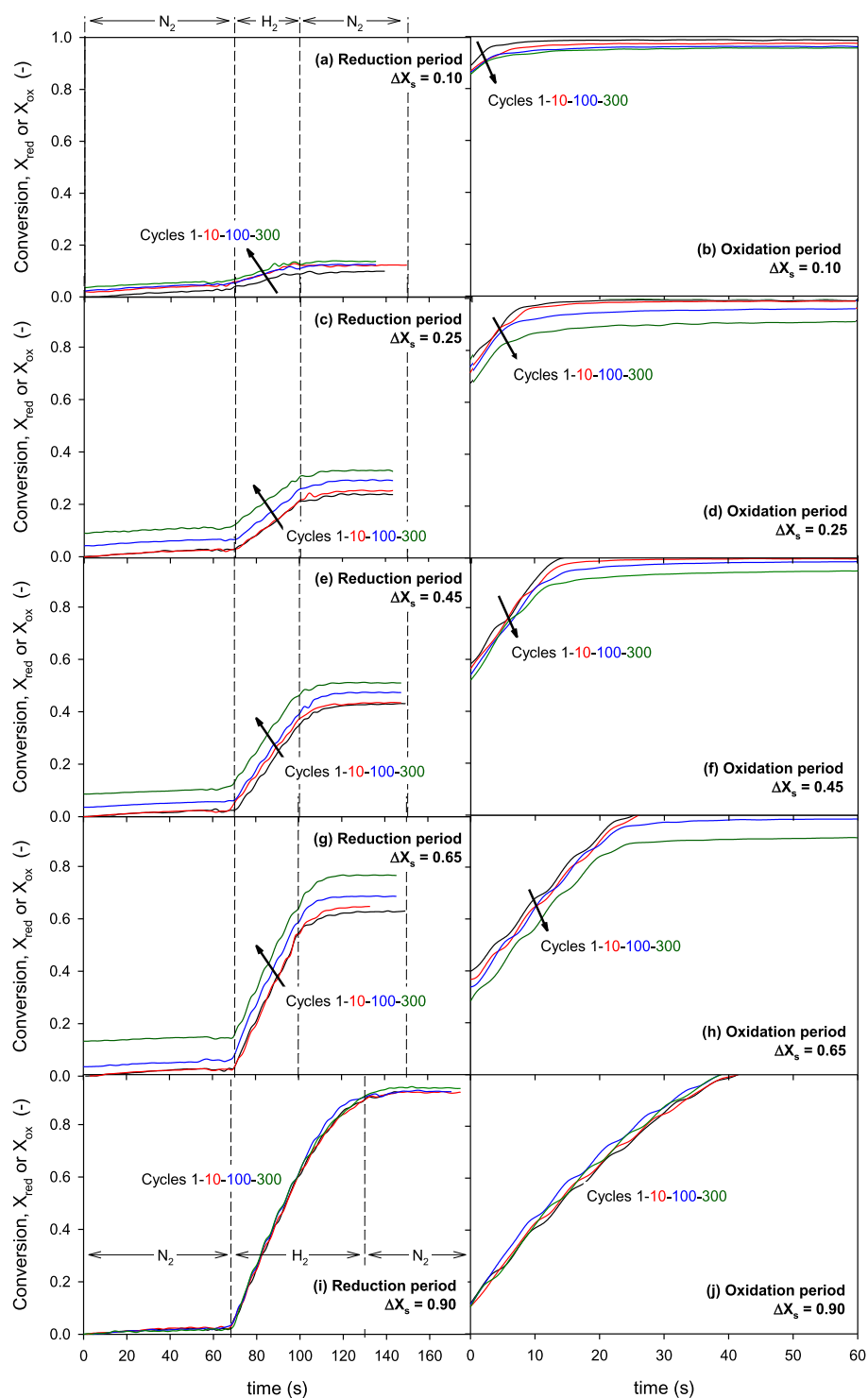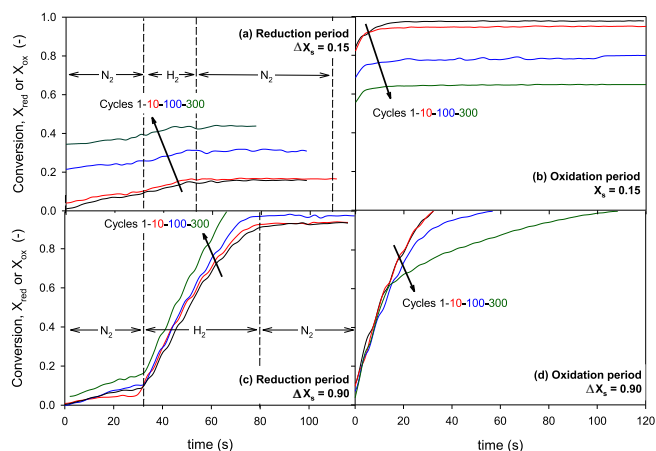
Fig. 2. Conversion vs time curves for reduction and oxidation periods for the 1st, 10th, 100th and 300th cycle. The oxygen carrier was highly oxidized after each redox cycle. Reaction temperature: 800 °C.

of the oxygen carrier was regenerated. A clear decrease in reactivity was then observed after a high number of redox cycles and a slight decrease in the degree of maximum oxidation was observed during the long-term test.

The observed behaviour suggests that copper speciation was affected by reaction conditions. Significant changes were detected by XRD analysis of the cycled samples and quantification of crystalline compounds is shown in Fig. 4. XRD patterns corresponding to TGA tests performed at 800 °C and 900 °C can be seen in Figures S3 and S4 of the

SM, respectively.

Copper was mostly present as CuO and $CuAl_2O_4$ in unreacted particles, which corresponds to the highest oxidized state of copper (Cu^{2+}). At 800 °C and $\Delta X_s = 0.1$, these same compounds were still the majority; but the presence of copper in the lower oxidation stage Cu^{1+} in the form of $CuAlO_2$ –at the expense of CuO– was important when the conversion variation increased to 0.25. A maximum fraction of $CuAlO_2$ was observed at $\Delta X_s = 0.45$. Then, it decreased in line with the increase in ΔX_s from 0.45 to 0.9. The presence of $CuAlO_2$ –not fully oxidized

Fig. 3. Conversion vs time curves for reduction and oxidation periods for the 1st, 10th, 100th and 300th cycle. The oxygen carrier was highly oxidized after each redox cycle. Reaction temperature: 900 °C.

compound– agrees with the decrease in maximum conversion after the oxidation stage with the redox cycles at intermediate values of ΔX_s; see Fig. 2. Interestingly, CuO increased with the increase in ΔX_s from 0.25 to 0.9 at the expense of the $CuAl_2O_4$ decrease. Eventually, low $CuAlO_2$ was found at $\Delta X_s = 0.9$, which agrees with the high and stable degree of oxidation after each redox cycle. The main difference at 900 °C was found at low ΔX_s values. In this case, the formation of copper aluminates was promoted, with $CuAlO_2$ being the major compound after successive redox cycles.

With regard to the alumina support, some δ-Al_2O_3 was formed from the γ-Al_2O_3 support during the calcining process. The chemical reaction during redox cycles promoted the formation of δ-Al_2O_3, which was the major alumina compound even at low ΔX_s values; see Fig. 4. γ-Al_2O_3 was fully converted to δ-Al_2O_3 when $\Delta X_s = 0.45$. Moreover, some α-Al_2O_3 appeared at higher ΔX_s values. At 900 °C, a deep transformation of γ-Al_2O_3 into α-Al_2O_3 was observed at both low and high ΔX_s values. α-Al_2O_3 was clearly promoted by the higher reaction temperature and high ΔX_s, which was accompanied by a decrease in the amorphous fraction.

When particles reacted at 800 °C, a progressive decrease in their porosity was observed as the variation in solids conversion increased; see Table 3. But porosity was relatively high (37.9 %) even when particles were highly reduced in every redox cycle ($\Delta X_s = 0.9$). Crushing strength was barely affected by the degree of reduction in the redox cycles. At 900 °C, the Cu14Al_ICB material showed good physical stability when the conversion variation was low, i.e. $\Delta X_s = 0.15$, as suggested by the low variation in crushing strength and porosity. However, the integrity of the particles could be compromised by high ΔX_s, as their

crushing strength decreased below 1 N [13,25].

Changes of the physico-chemical properties due to the thermochemical stress may modify the structure of the particles. Fig. 5 shows that unreacted particles present a clean external surface, derived from the preparation method. Particles with most of the copper introduced into the pores of γ-Al_2O_3 were obtained by the incipient wetness impregnation method used here. Then, samples cycled 300 times both at 800 °C and at 900 °C, and taken after the last oxidation stage, were examined by SEM-EDX. Fig. 6 show images for $\Delta X_s = 0.1$, 0.45 and 0.9 at 800 °C while Fig. 7 shows images for particles reacted at 900 °C. Figures for all ΔX_s values are found in Figures S5 and S6, SM.

The external surface of the particles was clearly affected by the conversion variation in every cycle, as well as the reaction temperature. At 800 °C (Fig. 6), no relevant differences were found compared to unreacted particles when $\Delta X_s = 0.1$, and most of copper was present inside the particles. The presence of copper on the external surface –confirmed by EDX analysis– progressively increased with increased conversion variation. SEM images were obtained by using backscattered electrons, and the presence of copper can be seen as bright spots. Thus, for $\Delta X_s = 0.9$ the external surface was covered by large grains of copper. The grains of copper inside the particles increased in size as ΔX_s

Table 3
Crushing strength and porosity of Cu14Al_ICB particles, fresh and after 300 cycles, with full oxidation during every redox cycle, with different variation in solids conversion.

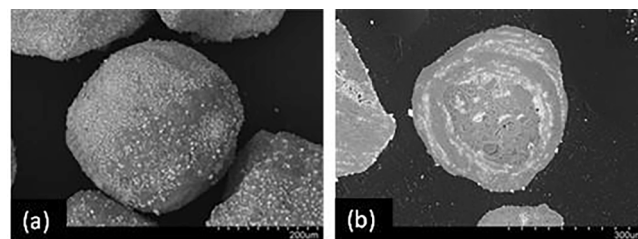| Sample	Temperature (°C)	Crushing strength (N)	Porosity (%)
Fresh	–	2.9 ± 0.6	50.0
$\Delta X_s = 0.10$	800	2.5 ± 0.6	53.1
$\Delta X_s = 0.25$	800	2.6 ± 0.7	48.8
$\Delta X_s = 0.45$	800	2.6 ± 0.6	47.1
$\Delta X_s = 0.65$	800	3.0 ± 0.8	45.0
$\Delta X_s = 0.90$	800	2.8 ± 0.8	37.9
$\Delta X_s = 0.15$	900	3.1 ± 0.9	53.7
$\Delta X_s = 0.90$	900	0.6 ± 0.2	61.5

Fig. 5. SEM images obtained with backscattered electrons of whole and cross-cut unreacted particles.
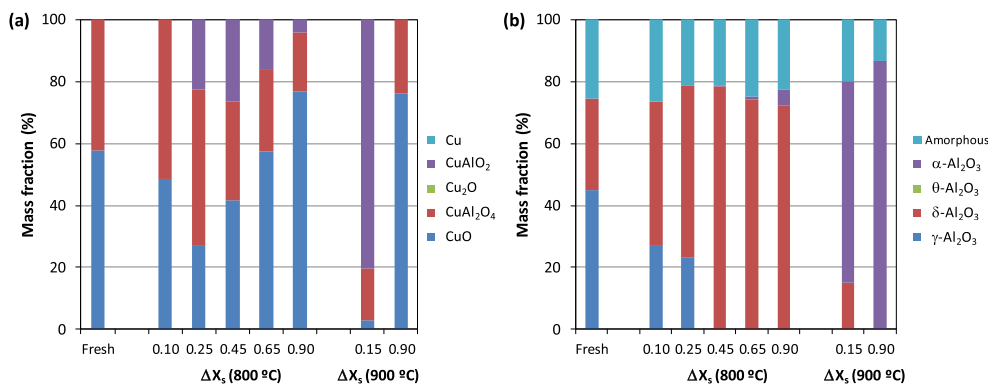

Fig. 4. Quantification of crystalline phases for fresh particles and material after 300 redox cycles as a function of the variation in conversion in each cycle: (a) copper-based compounds; (b) alumina compounds, including amorphous phase. The oxygen carrier was highly oxidized during each redox cycle.
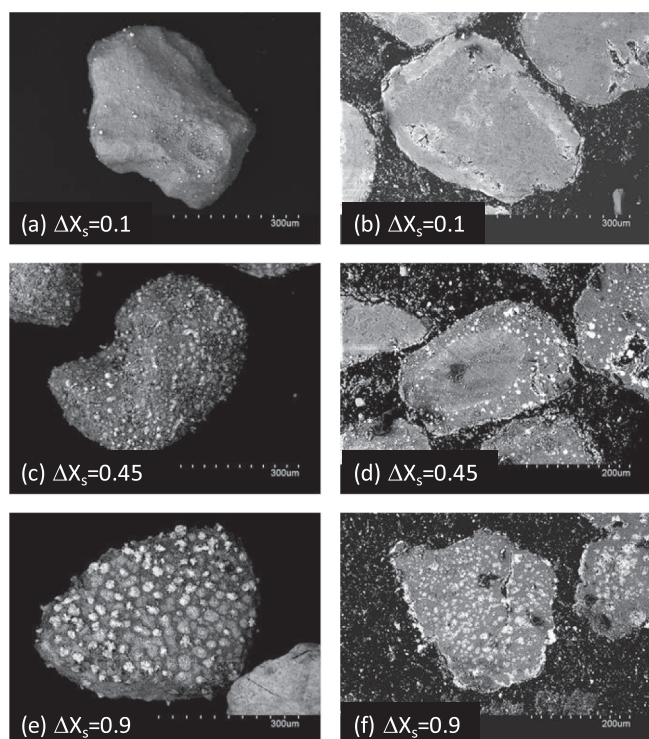
Fig. 6. SEM images obtained with backscattered electrons of whole and cross-cut particles as a function of conversion variation in the redox cycles. Particles highly oxidized in each redox cycle. Reaction temperature: 800 °C.
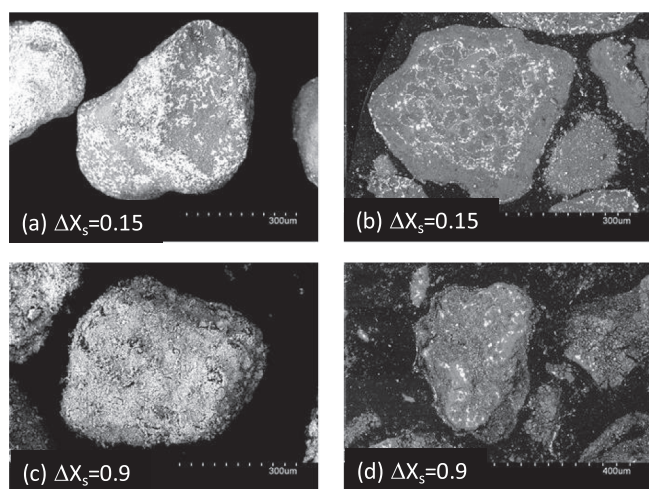

Fig. 7. SEM images obtained with backscattered electrons of whole and cross-cut particles as a function of the conversion variation in the redox cycles. Particles highly oxidized in each redox cycle. Reaction temperature: 900 °C.

increased. Large grains, likely formed by aggregation of copper, were observed in a corolla when ΔX_s was 0.25 and 0.45, while copper was uniformly distributed in the particle core. Copper sintering occurred within the whole particles at higher conversion variations, i.e. $\Delta X_s = 0.65$ and 0.95.

The migration of copper to the external surface was also found at 900 °C (Fig. 7); but the appearance of the external surface of the particles was uniform, suggesting that copper migration was of lesser importance and/or the copper was highly sintered at this temperature. At the lowest ΔX_s value, copper was concentrated inside the particle core, and a corolla with low copper content was observed. At higher values of the conversion variation, i.e. $\Delta X_s = 0.9$, the grains of copper

were homogeneously distributed throughout the whole particle.

3.2. Redox cycles with the highly reduced oxygen carrier

The tests described in Table 2 were performed to simulate the evolution in oxygen carrier properties when the oxygen carrier was highly reduced after every reduction semi-cycle. The evolution in solids conversion with the redox cycles, both at temperatures of 800 °C and 900 °C, is shown in Figures S7 and S8, SM. The conversion vs time curves for the 1st, 10th, 100th and 300th cycles are compared for all the tests performed at 800 °C and 900 °C, in Figs. 8 and 9.

When the oxygen carrier was fully reduced, the oxygen carrier showed excellent stability at 800 °C. The conversion variation was the same for the reduction and oxidation periods, and reactivity was very stable. Only a slight decrease was observed in conversion after the oxidation period when $\Delta X_s = 0.45$.

Excellent stability of reactivity was also observed at 900 °C at $\Delta X_s = 0.1$. However, oxidation conversion was negatively affected with the redox cycles at $\Delta X_s = 0.95$. This effect was also observed in Fig. 3(d) at $\Delta X_s = 0.90$. There, complete oxidation was promoted and a negative effect on reduction was not observed. Now, milder oxidation conditions were used, and a partial oxidation was only achieved; see Fig. 9(d). As a result, less oxygen was available for the next stage and reduction started
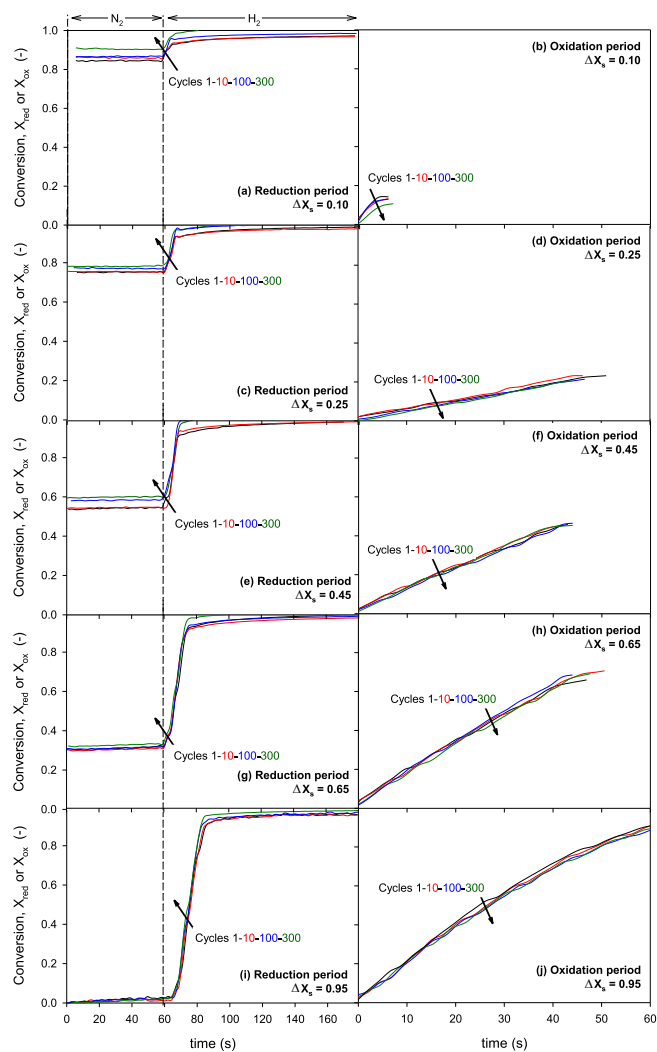

Fig. 8. Conversion vs time curves for reduction and oxidation periods for the 1st, 10th, 100th and 300th cycles. The oxygen carrier was highly reduced in each redox cycle. Reaction temperature: 800 °C.
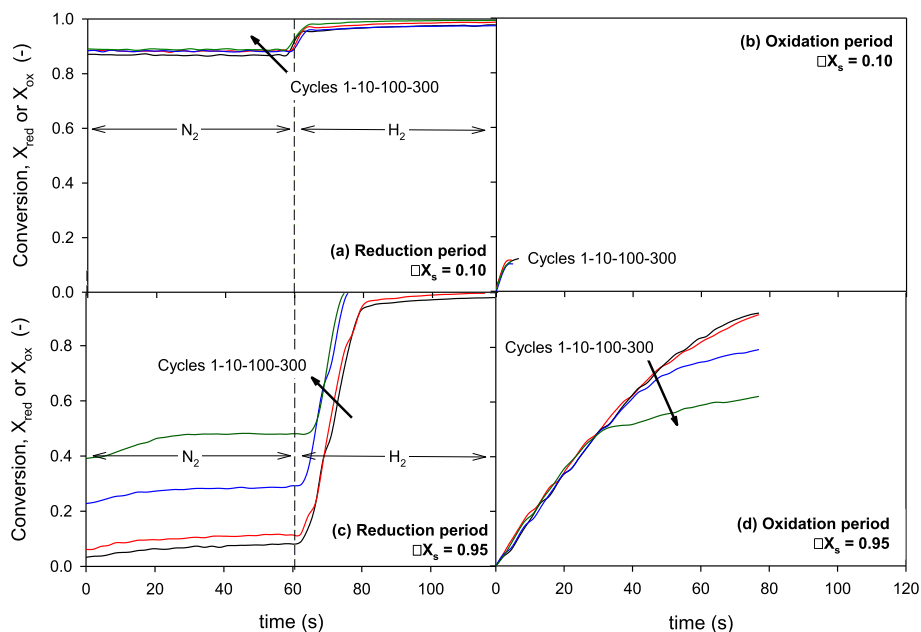
Fig. 9. Conversion vs time curves for reduction and oxidation periods for the 1st, 10th, 100th and 300th cycles. The oxygen carrier was highly reduced in each redox cycle. Reaction temperature: 900 °C.

with particles partially converted. Nevertheless, the reduction reactivity was not affected –i.e. same slope of the X_{red} vs. time curves. Another interesting difference between the results when oxygen carrier was highly oxidized (Figs. 2 and 3) or highly reduced (Figs. 8 and 9) was that the mass loss exhibited during the purge period in N_2 can no longer be seen, with the exception of the case at 900 °C and $\Delta X_s = 0.9$.

These results suggest that the copper speciation could be affected by the intensity of the reduction or oxidation. Thus, successive redox cycles modified the crystalline structure of the particles; see Fig. 10. XRD patterns corresponding to TGA tests performed at 800 °C and 900 °C can be seen in Figures S9 and S10 of the SM, respectively. At 800 °C, metallic Cu and Cu_2O were the main compounds up to ΔX_s values of 0.45, and these were progressively replaced by Cu^{2+} compounds, i.e. CuO and $CuAl_2O_4$, as ΔX_s approached unity, in accordance with the stoichiometry of the oxidized samples. Note that a sample composed only of Cu_2O would correspond to $\Delta X_s = 0.5$.

At 900 °C and $\Delta X_s = 0.1$, the main difference when compared to 800 °C was the presence of $CuAl_2O_4$, which suggests that the $CuO-Al_2O_3$ interaction increased with temperature. However, the only compound detected at $\Delta X_s = 0.95$ was Cu_2O. Subsequent oxidation to CuO was hindered, as shown in Fig. 9. Interestingly, $CuAlO_2$ was not observed in

any case, even when Cu_2O was present in the oxidized sample.

With regard to changes in the alumina support, γ-Al_2O_3 was progressively transformed into δ-Al_2O_3, θ-Al_2O_3 and α-Al_2O_3, which was promoted by the increase in the variation in solids conversion and reaction temperature. Thus, the amount of original γ-Al_2O_3 was marginal for $\Delta X_s > 0.1$, and a significant θ-Al_2O_3 fraction appeared. A low α-Al_2O_3 fraction was detected, but it became higher as ΔX_s increased. The appearance of θ-Al_2O_3 was promoted at 900 °C and $\Delta X_s = 0.1$, but most of the alumina was α-Al_2O_3 when ΔX_s was increased to 0.95. In the latter case, the amorphous phase was considerably lower than in all other cases.

Table 4 shows that the porosity of the particles decreased with the ΔX_s increase. So, the evolution of porosity at 800 °C was similar to what was found when oxygen carrier was fully oxidized in the oxidation period; see Table 3. Nevertheless, the intensity of the porosity decrease was higher when the oxygen carrier was highly reduced. In addition, the porosity of particles reacted at 900 °C was higher when compared to particles reacted at 800 °C.

The crushing strength values may be related to particle porosity. Thus, crushing strength increased as porosity decreased with ΔX_s. The only case where a deep reduction in the crushing strength parameter was
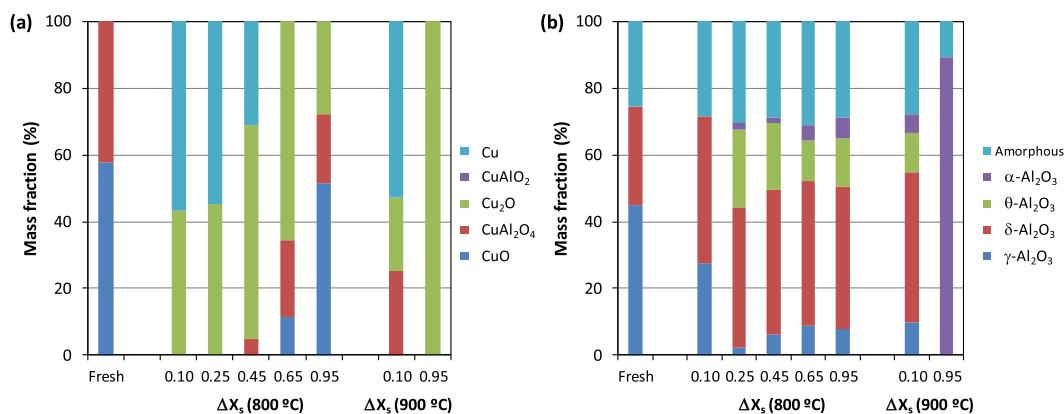

Fig. 10. Quantification of crystalline phases for fresh particles and material after 300 redox cycles as a function of the variation of conversion in each cycle: (a) copper-based compounds; (b) alumina compounds, including amorphous phase. The oxygen carrier was highly reduced in each redox cycle.

Table 4

Crushing strength and porosity of Cu14Al_ICB particles after 300 cycles, with full oxidation during every redox cycle, with different variation in solids conversion.

Sample	Temperature (°C)	Crushing strength (N)	Porosity (%)
$\Delta X_s = 0.10$	800	2.4 ± 0.7	50.5
$\Delta X_s = 0.25$	800	2.7 ± 0.8	49.9
$\Delta X_s = 0.45$	800	2.9 ± 0.6	45.7
$\Delta X_s = 0.65$	800	3.5 ± 1.2	37.8
$\Delta X_s = 0.95$	800	3.7 ± 1.2	28.7
$\Delta X_s = 0.10$	900	2.4 ± 0.5	53.0
$\Delta X_s = 0.95$	900	1.5 ± 0.4	45.0

observed was when particles reacted at 900 °C and $\Delta X_s = 0.95$, which may be related to a strong change in the crystalline phases during the redox cycles. Nevertheless, the crushing strength value was above the threshold value of 1 N to be suitable for its use in a CLC unit [13,25].

In general, particle integrity was maintained even when the conversion variation was high. This fact was confirmed by SEM images. As examples, images for $\Delta X_s = 0.1$ and 0.9 are shown in Figs. 11 and 12 for reacting temperatures of 800 and 900 °C, respectively. Figures for all ΔX_s values are found in Figures S11 and S12, SM. Again, migration of copper to the external surface of the particles was observed after the redox cycles, and it was promoted by ΔX_s. In fact, small grains of copper at low ΔX_s values and homogeneous distribution of copper at high ΔX_s values were observed on the particle surface at both 800 °C and 900 °C. In addition, copper accumulation in grains inside the particle was observed as ΔX_s increased. However, the nucleus-corolla structure detected when particles were fully oxidized –Figs. 6 and 7– is now not observed. This fact suggests that the homogeneity of the particle was more easily preserved when particles were highly reduced in every redox cycle, which can positively affect to the integrity of the particles.

3.3. Unravelling reaction mechanisms for copper speciation

Results obtained under different conditions can shed light on the relevance of possible reactions occurring during the reduction and oxidation periods, summarized in Table 5. Figure S13 of the SM shows an Ellingham diagram corresponding to the potential reactions involving the Cu14Al_ICB oxygen carrier. Fig. 13 represents these reactions including conclusions from this discussion section. After calcination, copper was present in both CuO and $CuAl_2O_4$, which may have been formed by reaction (R1). The period in N_2 before reduction with H_2 was characterized by the generation of gaseous oxygen through the
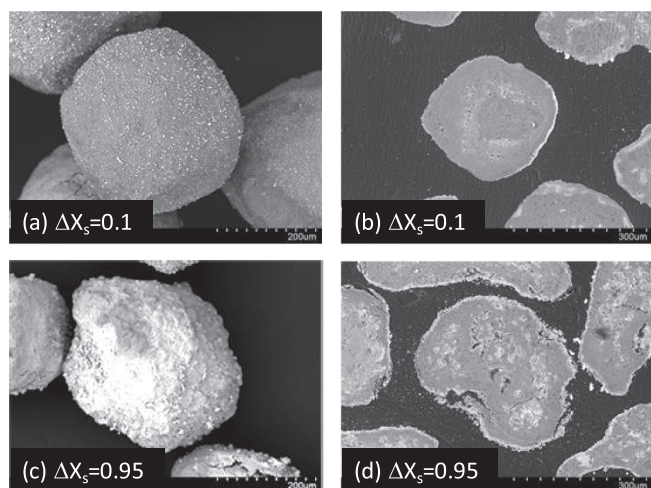

Fig. 11. SEM images obtained with backscattered electrons of whole and cross-cut particles as a function of the conversion variation in the redox cycles. Particles fully reduced in each redox cycle. Reaction temperature: 800 °C.
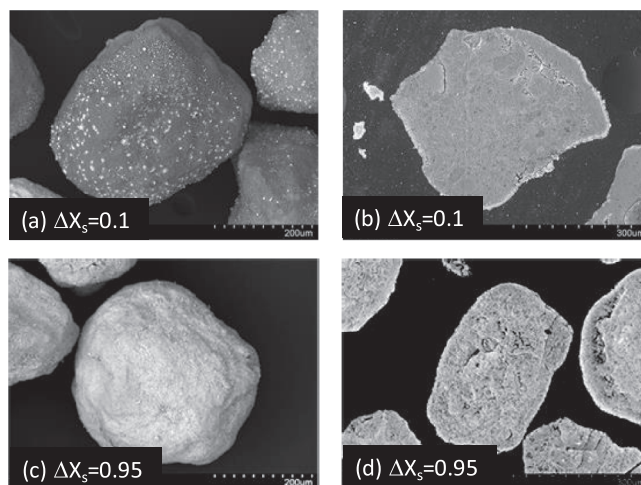

Fig. 12. SEM images obtained with backscattered electrons of whole and cross-cut particles as a function of the conversion variation in the redox cycles. Particles fully reduced in each redox cycle. Reaction temperature: 900 °C.

Table 5

Proposed reactions involving the Cu14Al_ICB-oxygen carrier during reduction and oxidation semi-cycles.

Reaction		Mainly occurring in	
		reduction	oxidation
$CuO + Al_2O_3 \rightarrow CuAl_2O_4$	(R1)	X	X
$2\,CuO \rightarrow Cu_2O + 0.5\,O_2$	(R2)	X	
$2\,CuAl_2O_4 \rightarrow 2\,CuAlO_2 + Al_2O_3 + 0.5\,O_2$	(R3)	X	
$CuO + H_2 \rightarrow Cu + H_2O$	(R4)	X	
$CuAl_2O_4 + H_2 \rightarrow Cu + Al_2O_3 + H_2O$	(R5)	X	
$2\,CuO + H_2 \rightarrow Cu_2O + H_2O$	(R6)	X	
$Cu_2O + H_2 \rightarrow 2\,Cu + 2\,H_2O$	(R7)	X	
$2\,CuAl_2O_4 + H_2 \rightarrow 2\,CuAlO_2 + Al_2O_3 + H_2O$	(R8)		
$2\,CuAlO_2 + H_2 \rightarrow 2\,Cu + Al_2O_3 + H_2O$	(R9)		
$Cu + 0.5\,O_2 \rightarrow CuO$	(R10)		X
$2\,Cu + 0.5\,O_2 \rightarrow Cu_2O$	(R11)		X
$Cu_2O + 0.5\,O_2 \rightarrow 2\,CuO$	(R12)		X
$2\,CuAlO_2 + 0.5\,O_2 \rightarrow CuAl_2O_4 + CuO$	(R13)		
$Cu_2O + Al_2O_3 \rightarrow 2\,CuAlO_2$	(R14)		
$2\,CuO + Al_2O_3 \rightarrow 2\,CuAlO_2 + 0.5\,O_2$	(R15)	X	
$4\,CuAl_2O_4 \rightarrow 2\,Cu_2O + 4\,Al_2O_3 + O_2$	(R16)		

oxygen uncoupling mechanism, and a slight increase in conversion was observed. CuO and $CuAl_2O_4$ were potentially the oxides taking part in this reaction; see reactions (R2) and (R3). Cu_2O and $CuAlO_2$ are the products of the oxygen uncoupling reactions, respectively.

$CuAlO_2$ was accumulated only in some specific cases. Possible reactions for $CuAlO_2$ formation are (R3), (R8) or (R14). The interpretation of these results may offer some clue about the route by which this compound is mainly formed. Reactions (R3) and (R8) involve the presence of $CuAl_2O_4$, while (R14) needs Cu_2O and a solid-state reaction with Al_2O_3. Cu_2O was a main compound when the oxygen carrier was highly reduced (see Fig. 10), but $CuAlO_2$ was not observed. Therefore, it is believed that reaction (R14) is of less importance for the formation of $CuAlO_2$. The $CuAlO_2$ formation caused the decrease in the oxidation conversion observed in some cases in Figs. 2 and 3. Formation of $CuAlO_2$ by reduction of $CuAl_2O_4$ –reaction (R8)– would cause a quick accumulation of $CuAlO_2$. This was not the case because the decrease in the oxidation conversion was gradual, which suggests that $CuAlO_2$ formation was also gradual. Therefore, $CuAlO_2$ was likely formed by the oxygen uncoupling reaction (R3), which was promoted by temperature. In addition, reaction (R15) may be an alternative route for $CuAlO_2$ formation, which was relevant to justify its presence in a previous work [16]. However, this reaction can be considered as the concatenation of reactions (R1) and (R3) or (R2) and (R14). In this sense, reaction (R3)
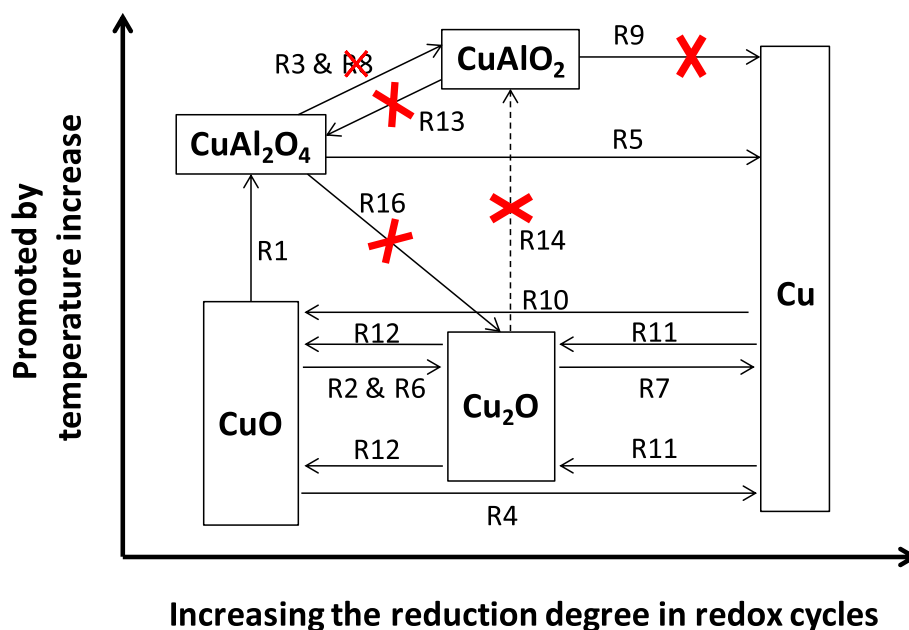
Fig. 13. Picture of the proposed reactions involving the Cu14Al_ICB-oxygen carrier during reduction and oxidation semi-cycles.

would determine the accumulation of $CuAlO_2$. Note that once $CuAlO_2$ was formed, its oxidation to $CuAl_2O_4$ was hindered. Therefore, $CuAlO_2$ can be considered as an inactive compound both for reduction and oxidation.

For the reduction in the presence of H_2, different routes could be determined depending on the reaction temperature and oxygen carrier characteristics, including direct reduction to Cu –reactions (R4) and (R5)– or a cascade mechanism with Cu_2O or $CuAlO_2$ as intermediate compounds –reactions (R6)-(R9):

- For the reduction of CuO to Cu, here there is not evidences to determine the preferred route. It would be necessary to characterize the material after the reduction half-cycle, rather than after the oxidation half-cycle as shown in the Figs. 4 and 10. This task was not the main objective of this work, but some information can be considered from previous results [16]. It was determined that direct reduction route –reaction (R4)– was dominant at 800 °C, but CuO reduction in two steps –reactions (R6) and (R7)– was relevant at 900 °C.
- The reduction of $CuAl_2O_4$ to $CuAlO_2$ by H_2 –reaction (R8)– was ruled out in the previous discussion. In addition, $CuAlO_2$ was difficult to be reduced by H_2 –reaction (R9). Therefore, the direct reduction to Cu –reaction (R5)– would be the most likely route.

During the regeneration period, Cu may have been oxidized both via a direct route –reaction (R10)– or via a cascade mechanism, with Cu_2O being an intermediate compound –reactions (R11)-(R12). During the oxidation of the oxygen carrier being highly reduced it was observed the co-existence of Cu and Cu_2O at low ΔX_s values, but Cu_2O and CuO at high ΔX_s values. These results suggest that the cascade mechanism may be preferred at 800 °C. However, the direct oxidation of Cu to CuO, and then the formation of $CuAl_2O_4$, is promoted by temperature, as $CuAl_2O_4$ was observed at $\Delta X_s = 0.1$ and 900 °C but not at 800 °C in Fig. 10. Anyway, the cascade mechanism still may be of relevance at high temperature, mostly at $\Delta X_s = 0.95$, likely due to a higher sinterization of copper grains inside the particle.

$CuAl_2O_4$ was a minor compound when ΔX_s was high. This fact suggest that $CuAl_2O_4$ was formed by solid-state reaction of CuO and Al_2O_3 –reaction (R1)– instead of the direct formation through oxidation of Cu in the presence of Al_2O_3, and it is promoted when the oxygen carrier was

highly oxidized; see Fig. 4. The relative fraction of CuO and $CuAl_2O_4$ after oxidation would depend on the ΔX_s value. In addition, the possible oxidation of $CuAlO_2$ is described by reaction (R13), but it is believed that this reaction does not occur in a relevant extension.

3.4. Comparison with results obtained in CLC units

For comparison purposes and to validate the method developed in TGA, the results achieved during 570 h of continuous operation with the Cu14Al_ICB oxygen carrier in CLC units at different temperatures and oxygen carrier-to-fuel ratios are considered. In general, the use of Cu14Al_ICB in CLC units showed good fluidization properties, including avoidance of agglomeration and low attrition rate at suitable conditions; no trend to carbon deposition; and high enough reactivity and oxygen transport capacity to achieve complete combustion of gaseous fuels even at high ΔX_s.

Most of experience in CLC units with Cu14Al_ICB material was gained under conditions promoting high oxidation of the oxygen carrier in the AR because this reactor is usually over-sized compared to the FR. This condition was simulated by the tests described in Table 1. Taking this into consideration, the results obtained in this work can be compared to results from CLC unit operation:

- The reaction temperature itself induced changes in the solid structure or phases. More particularly, higher temperature promoted the transition from γ-Al_2O_3 to α -Al_2O_3. However, this modification in the crystal structure of Al_2O_3 took place at a lower temperature than its transformation (1150 °C). This suggests that the presence of copper promotes this transformation in alumina, most likely during Al_2O_3 generation by reactions (R3) and (R5) of $CuAl_2O_4$ [26]; earlier it was deduced that other reactions with Al_2O_3 as a product, such a partial reduction of $CuAl_2O_4$ with H_2 -reaction (R8)- and reduction of $CuAlO_2$ -reaction (R9)- were of lower relevance. The formation of α-Al_2O_3 by these reactions may be promoted at 900 °C, while δ- or θ-Al_2O_3 is favoured at 800 °C. In addition, the crystallinity of the support increases with temperature. These facts affect particle integrity, i.e. crushing strength, and eventually particle fragmentation, attrition rate and lifetime in a CLC unit. For example, crushing strength was 2.8 and 0.6 N at 800 °C and 900 °C, respectively, at high ΔX_s values, which can be related to the estimated lifetime values of

2400 h [27] and < 400 h [12] achieved during operation in a CLC unit. It is important to note that changes in crystallinity at 900 °C were less significant at low ΔX_s values, which agrees with the lower effect of redox cycles on crushing strength obtained in this work and during CLC operation at high oxygen carrier-to-fuel ratios [16]. Thus, the crushing strength of the particles reacted at 900 °C and ΔX_s = 0.15 was 3.1 N, which can be compared to the 0.6 N obtained for ΔX_s = 0.9.

- The thermal shock related to the rapid heating or cooling of particles entering the AR or FR may also affect the mechanical performance of solid particles [28], but it is believed to be of less importance in CLC because the temperatures in both reactors would not be very different with Cu-based materials [20]. This justifies performing redox cycles at the same temperature for reduction and oxidation.

- Copper migration to the particle surface was favoured at 800 °C. Formation of nodules of copper aggregates in the core of the particle was favoured at 900 °C, which reduced migration of copper to the particle surface. Copper on the surface can be detached from the particle by abrasion, which is linked to the loss of copper observed in CLC units. Thus, the loss of copper in the particle was higher at 800 °C (e.g. from 14 to 10 wt% CuO [27]), than at 900 °C (from 14 to 13 wt% CuO [12]).

- Copper migration was also affected by ΔX_s. Copper migration was highly favoured by increasing ΔX_s at 800 °C. This agrees with the results obtained in a CLC unit, where the loss of CuO was between 14 wt% and 12.1 wt% at ΔX_s = 0.1–0.2 [16], but decreased to 10 wt% at ΔX_s = 0.5–0.1 [27]. Copper migration was of less importance at 900 °C, and therefore, CuO loss was lower; e.g. remaining CuO was 13.8 wt% at ΔX_s = 0.1–0.2 [16] and 13 wt% CuO at ΔX_s = 0.8–1 [12]. Note that copper loss may be also affected by the preparation method. For example, particles prepared by wet impregnation have initially a higher amount of copper in the particle surface, which is easily detached during the firsts hours of operation [29].

- Copper speciation was affected by both reaction temperature and ΔX_s. In general, the interaction of CuO with alumina at ΔX_s = 0.9 was lower than at ΔX_s = 0.1. This suggests that the formation of copper aluminates is hindered when the copper is highly reduced by reactions (R4) or (R5). This fact was also observed for Ni-based materials impregnated on α-Al$_2$O$_3$ [30]. However, some CuAl$_2$O$_4$ was still formed following reaction (R1). Interestingly, CuAlO$_2$ was formed at 800 °C and intermediate ΔX_s values, which agrees with results from CLC units [12,16].

- Interestingly, CuAlO$_2$ was highly accumulated when particles reacted at 900 °C and ΔX_s = 0.1, and high oxidation was promoted; see Fig. 4. This was also observed in a CLC unit when the oxygen carrier to fuel ratio was maintained at high values [16]. As a consequence, the fuel conversion was not complete. This fact reveals the importance of temperature on the reaction of existing CuAl$_2$O$_4$ to form CuAlO$_2$ via reactions (R3), and consequently the progressive accumulation of CuAlO$_2$. The absence of CuAlO$_2$ when ΔX_s = 0.1 at 800 °C suggests that CuAlO$_2$ formation takes place more slowly than other reactions. Thus, CuAlO$_2$ increased as ΔX_s increased because the residence time of solids in the FR increased. A maximum of CuAlO$_2$ was observed for ΔX_s = 0.45. At higher ΔX_s values, reduction to Cu was promoted, thus decreasing the interaction of copper with alumina.

- Conditions promoting CuAlO$_2$ formation should be avoided during CLC operation. On the contrary, unreactive CuAlO$_2$ accumulated in the particles because it was difficult for it to be reduced or oxidized by reactions (R9) or (R13).

From the discussion above, the method developed in TGA is able to identify the physico-chemical changes that the oxygen carrier undergoes in a CLC unit during hundreds of redox cycles. One important and specific aspect of continuous CLC pilot plants is the distribution of residence time of solid particles in the fuel reactor, which entails a distribution of conversion of the particles at the outlet stream. However, the consistency between the results obtained in TGA and in continuous CLC facilities reveals that this factor does not significantly affect the physico-chemical changes experienced by the oxygen carrier particles. This is because in continuous CLC units operating for many hours at steady state, the oxygen carrier is subjected to hundreds of redox cycles and under these conditions the conversion of any particle in the fuel reactor is close to a mean value of solids conversion, which is the one that is compared with the solids conversion set in the tests performed in TGA.

3.5. Practical implications for using the oxygen carrier in CLC

The results obtained in the TGA tests are now discussed considering the different operating conditions that can exist in a CLC unit, which was the main objective of this work.

At a glance, the main results achieved during the physico-chemical characterization of the aged material are summarized in Table S2, SM. These results can also be observed in the Fig. 14, where the following indicators are qualitatively evaluated: redox stability, reactivity, fixing Cu, crushing strength, Al$_2$O$_3$ changes, Cu aluminates and intensity of the amorphous phase. Modifications in physico-chemical properties were related to changes in the support, from γ to α alumina, as well as to modifications in Cu speciation, with the appearance of new phases as CuO in the oxidized form, and Cu$_2$O, Cu and CuAlO$_2$ in the reduced form. These changes depended on the reaction temperature and the variation in solids conversion, which affected the lifetime determined under each operating condition.

The oxygen carrier-to-fuel ratio and solids circulation rate in a CLC unit is inversely proportional to the variation in solids conversion, ΔX_s -see Eq. (1)-, as it is shown in Fig. 15. Chemical stress in a CLC unit is related to the variation in solids conversion between AR and FR, ΔX_s, which has been simulated in the TGA tests. The active component in the oxygen carrier is oxidized to $X_{ox,AR}$ in AR (conversion of solids at the FR inlet, $X_{ox,inFR}$), while is reduced to $X_{ox,FR}$ in FR (with $X_{ox,outFR} = X_{ox,FR}$ and $X_{ox,FR.} < X_{ox,AR}$). Thus, $\Delta X_s = X_{ox,AR} - X_{ox,FR}$. Fig. 15 was designed to visualize the relationship between different design and operating parameters of a CLC unit, namely $X_{ox,inFR}$, $X_{ox,inAR}$, ΔX_s, solids circulation rate and solids inventory. The methodology proposed by Abad et al. [20] was used to calculate the minimum solids inventory as a function of $X_{ox,inFR}$ and ΔX_s. It is observed that high ΔX_s values are related to low φ values, and vice versa. In addition, the solids inventory in both reactors (FR and AR) increases as ΔX_s increases for a fixed value of $X_{ox,inFR}$. Interestingly, high oxidation degree in the AR is promoted by high solids inventory in this reactor. On the contrary, high reduction degree of the oxygen carrier in the fuel reactor is promoted by high solids inventory values in the FR, as well as low solids inventory in the AR. Therefore, an excess of solids in the AR promotes conditions tested in Table 1, but an oversized FR or one AR with low solids inventory promotes the conditions tested in Table 2, i.e. high reduction of solids in the FR. These conditions may be related to the qualification shown in Fig. 14.

In order to preserve the good mechanical properties of the material, the oxygen carrier can be used under the following conditions:

- At 800 °C, φ higher than 10 or lower than 1.2 is recommended when the degree of oxidation in the AR is high. On the contrary, a broad range of φ values could be explored.
- At 900 °C, low φ values are recommended when the degree of oxidation in the AR is high. Otherwise, high φ values would be advisable.

However, experience in CLC has been mostly limited to the case where the oxygen carrier is highly regenerated after the oxidation semicycle, although this would not be the case in an industrial unit. For example, some results were achieved with low residence time of solids in the AR in the 120 kW CLC unit at Vienna University of Technology, thus limiting the degree of oxidation to low values [31], but a
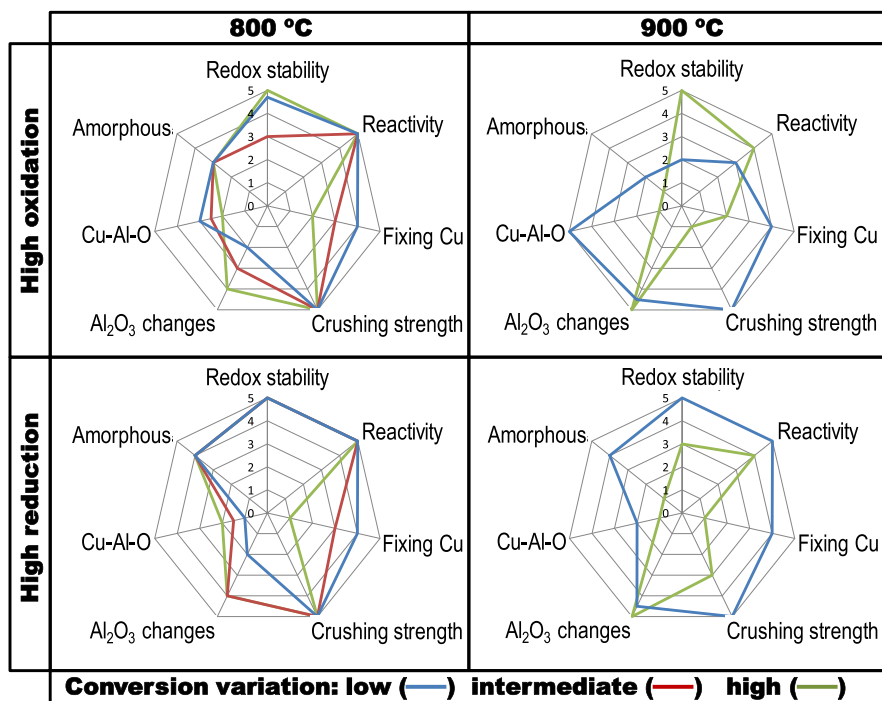
Fig. 14. Qualitative evaluation of several indicators as a function of the reaction temperature, the degree of oxidation and the variation of the solids conversion.
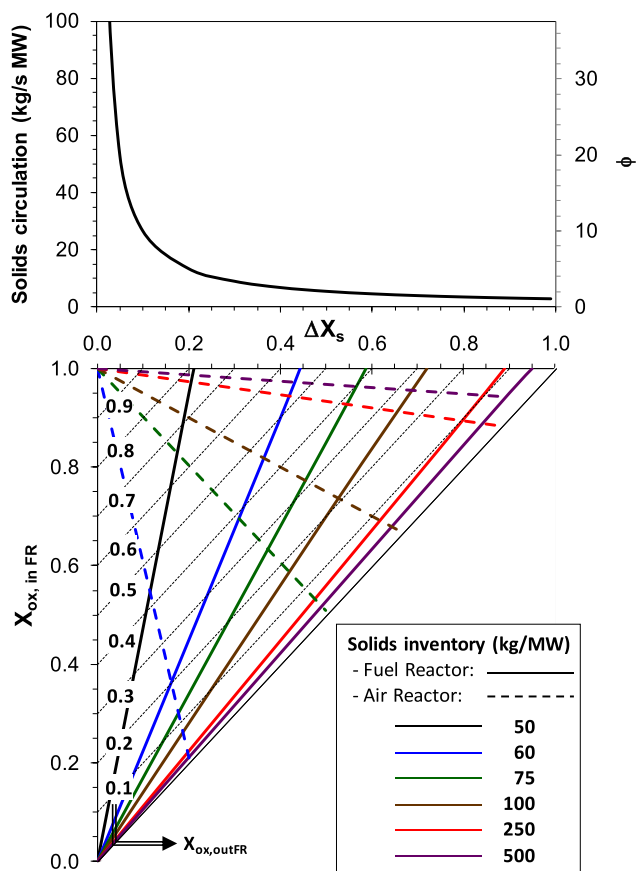

Fig. 15. Solids circulation rate and minimum solids inventory in the fuel and air reactors for Cu14Al_ICB as a function of the variation of the solids conversion (ΔX_s) and the oxidation conversion of solids at the fuel reactor inlet ($X_{ox, inFR}$). The corresponding conversion of solids at the fuel reactor outlet ($X_{ox,outFR}$) is also depicted.

characterization of the oxygen carrier material under this condition is not available. It can also happen in Chemical looping reforming (CLR) [32] and Chemical looping gasification (CLG) processes [33], where the air-to-fuel ratio is kept at low values to achieve partial oxidation of the fuel.

The tests in Table 2 were an attempt to replicate its behaviour in such a case, i.e. 120 kW CLC unit, CLR or CLG. Important practical implications can be extracted from these results:

- At 800 °C, transformation of alumina to θ-Al$_2$O$_3$ and α-Al$_2$O$_3$ was promoted by the increase in ΔX_s. This transformation took place at a temperature lower than the transition temperature from δ-Al$_2$O$_3$ to θ-Al$_2$O$_3$ (1080 °C) and from θ-Al$_2$O$_3$ to α-Al$_2$O$_3$ (1150 °C) [34], suggesting the presence of copper –or more specifically CuAl$_2$O$_4$– promoted this transformation. However, crystallinity was low, which resulted in high crushing strength values, even higher than those of the original particles. At 900 °C, α-Al$_2$O$_3$ only was significant at high ΔX_s values, resulting in high crystallinity and a decrease in crushing strength. Nevertheless, crushing strength was higher (1.5 N) than when particles were highly oxidized (0.6 N).
- The interaction of copper with alumina was lower when the oxygen carrier was highly reduced. Thus, most of copper was in the form of Cu, Cu$_2$O or CuO, depending on the degree of oxidation. No CuAlO$_2$ was observed, which suggests that all the copper would have been active for the oxygen transfer. With regard to reactivity, it is remarkable to note a decrease in regeneration capability at 900 °C and $\Delta X_s = 0.95$, which was limited to oxidation to Cu$_2$O. This will cause a decrease in the oxygen transfer capability of the material and incomplete fuel conversion. Therefore, high φ and low ΔX_s values would be recommended at 900 °C.
- Copper migration was very limited at low ΔX_s values, which suggests copper loss would be low when operating with high φ values in a CLC unit.

Given the excellent mechanical stability of particles when the degree of oxidation was limited in the AR, the use of Cu14Al_ICB material under such conditions deserves to be explored in a CLC unit in the future. It might be interesting to explore the behaviour of this oxygen carrier at

900 °C, but maintaining ΔX_s at low values. Moreover, this oxygen carrier could be used in the CLR or CLG processes under such conditions.

These are the main conclusions of applying the method developed in this work for the Cu14Al_ICB oxygen carrier. However, the use of this method for other oxygen carriers would not imply that they had to operate under the same conditions as the Cu14Al_ICB oxygen carrier in order to optimize their mechanical behaviour in continuous CLC processes. As future work, it would be very interesting to try to validate this method for existing oxygen carriers based on other metal oxides [30,35] and supports [36] and developed by other methods of preparation [37–39]. In order to do this, it will be also necessary to have extensive characterization data of used samples from experimental campaigns carried out in continuous CLC plants, which are often not available.

Results shown in this work were achieved by performing hundreds of redox cycles in a TGA under well-established conditions. Several tests were done keeping constant the reaction temperature and the variation of the solids conversion. Even though it is a hard work, the effort it represents is much less than what should be done in a CLC unit to obtain the same conclusions. Thus, tests in a TGA will guide future development of oxygen carrier materials by defining the operating conditions that are worth evaluating in a CLC unit to maximize material usage. In this way, the scaling up of the process can be accelerated obtaining reliable results with a lower effort.

4. Conclusions

A method is described to identify promising oxygen carriers for use in CLC units, as well as to determine most favourable conditions in a CLC unit to evaluate the effect of operating time on the mechanical integrity of the oxygen carrier particles. The method was based on the ageing of an oxygen carrier material in a TGA during hundreds of redox cycles under well-defined operating conditions, such as reaction temperature, variation in solids conversion and oxidation state after the completion of each redox cycle.

The method was evaluated with a well-known Cu-based material impregnated on Al_2O_3, which was used for>500 h in different CLC units. The results achieved by applying the method were validated against results extracted during CLC operation when the oxygen carrier was highly regenerated after the oxidation semi-cycle. The method performed in the TGA was able to predict the variations in physico-chemical properties of the Cu14Al_ICB oxygen carrier particles observed in CLC units. More important results were related to the evolution of crushing strength, copper migration and copper speciation with redox cycles. In addition, new operating conditions were identified for use in a CLC unit in order to improve the lifetime of the material at high temperature, i.e. 900 °C. These conditions take into consideration the limitation of the degree of oxidation in the AR.

By determining suitable operating conditions through this novel method, the effort required to obtain reliable results during the operation of a CLC unit may be reduced. The scale-up of CLC technology will eventually be promoted by boosting the identification of oxygen carrier materials and suitable operation conditions for testing at industrial scale.

Declaration of Competing Interest

The authors declare that they have no known competing financial interests or personal relationships that could have appeared to influence the work reported in this paper.

Acknowledgements

Appendix A. Supplementary data

Supplementary data to this article can be found online at https://doi.org/10.1016/j.cej.2021.132602.

References

[1] IEAGHG, Carbon Capture and Storage and the Sustainable Development Goals, 2020-14, December 2020.

[2] F. Petrakopoulou, G. Tsatsaronis, Can carbon dioxide capture and storage from power plants reduce the environmental impact of electricity generation? Energy Fuels 28 (8) (2014) 5327–5338.

[3] T. Mendiara, F. García-Labiano, A. Abad, P. Gayán, L.F. de Diego, M.T. Izquierdo, J. Adánez, Negative CO2 emissions through the use of biofuels in chemical looping technology: A review, Appl. Energy 232 (2018) 657–684.

[4] J. Adánez, A. Abad, Chemical-looping combustion: Status and research needs, Proc. Combust. Inst. 37 (4) (2019) 4303–4317.

[5] J. Adánez, A. Abad, T. Mendiara, P. Gayán, L.F. de Diego, F. García-Labiano, Chemical looping combustion of solid fuels, Prog. Energy Combust. Sci. 65 (2018) 6–66.

[6] A. Fossdal, O. Darell, A. Lambert, E. Schols, E. Comte, R. Leenman, R. Blom, Study of dimensional changes during redox cycling of oxygen carrier materials for chemical looping combustion, Energy Fuels 29 (1) (2015) 314–320.

[7] A. Lambert, E. Comte, D. Marti, T. Sozinho, S. Bertholin, H. Stainton, M. Yazdanpanah, On the mechanisms of oxygen carrier degradation during multiple CLC cycles, Proc. 6th High Temperature Solid Looping Network Meeting, Milan, Italy, 2015.

[8] S.C. Bayham, R. Breault, E. Monazam, Particulate solid attrition in CFB systems – An assessment for emerging technologies, Powder Technol. 302 (2016) 42–62.

[9] A. Cabello, A. Abad, P. Gayán, F. García-Labiano, L.F. de Diego, J. Adánez, Increasing energy efficiency in chemical looping combustion of methane by in-situ activation of perovskite-based oxygen carriers, Appl. Energy 287 (2021), 116557.

[10] S.C. Bayham, R. Breault, E. Monazam, Applications of tribology to determine attrition by wear of particulate solids in CFB systems, Powder Technol. 316 (2017) 59–68.

[11] A. Lyngfelt, A. Brink, Ø. Langørgen, T. Mattisson, M. Rydén, C. Linderholm, 11,000 h of chemical-looping combustion operation - Where are we and where do we want to go? Int. J. Greenhouse Gas Control 88 (2019) 38–56.

[12] C.R. Forero, P. Gayán, F. García-Labiano, L.F. de Diego, A. Abad, J. Adánez, High temperature behaviour of a CuO/γAl2O3 oxygen carrier for chemical-looping combustion, Int. J. Greenhouse Gas Control 5 (2011) 659–667.

[13] A. Cabello, P. Gayán, F. García-Labiano, L.F. de Diego, A. Abad, J. Adánez, On the attrition evaluation of oxygen carriers in Chemical Looping Combustion, Fuel Process. Technol. 148 (2016) 188–197.

[14] I. Adánez-Rubio, A. Abad, P. Gayán, L.F. de Diego, J. Adánez, CLOU process performance with a Cu-Mn oxygen carrier in the combustion of different types of coal with CO2 capture, Fuel 212 (2018) 605–612.

[15] M. Schmitz, C. Linderholm, Chemical looping combustion of biomass in 10- and 100-kW pilots – Analysis of conversion and lifetime using a sintered manganese ore, Fuel 231 (2018) 73–84.

[16] M.T. Izquierdo, F. García-Labiano, A. Abad, A. Cabello, P. Gayán, L.F. de Diego, J. Adánez, On the optimization of physical and chemical stability of a Cu/Al2O3 impregnated oxygen carrier for chemical looping combustion, Fuel Process. Technol. 215 (2021), 106740.

[17] L.F. de Diego, P. Gayán, F. García-Labiano, J. Celaya, A. Abad, J. Adánez, Impregnated CuO/Al2O3 oxygen carriers for chemical-looping combustion: Avoiding fluidized bed agglomeration, Energy Fuels 19 (2005) 1850–1856.

[18] A. Cabello, P. Gayán, A. Abad, L.F. de Diego, M.T. Izquierdo, A. Scullard, G. Williams, J. Adánez, Long-lasting Cu-based oxygen carrier material for industrial scale in Chemical Looping Combustion, Int. J. Greenhouse Gas Control 52 (2016) 120–129.

[19] T. Mattisson, M. Keller, C. Linderholm, P. Moldenhauer, M. Rydén, H. Leion, A. Lyngfelt, Chemical-looping technologies using circulating fluidized bed systems: Status of development, Fuel Process. Technol. 172 (2018) 1–12.

[20] A. Abad, J. Adánez, F. García-Labiano, L.F. de Diego, P. Gayán, J. Celaya, Mapping of the range of operational conditions for Cu-, Fe-, and Ni-based oxygen carriers in chemical-looping combustion, Chem. Eng. Sci. 62 (1-2) (2007) 533–549.

[21] C. Chung, L. Qin, V. Shah, L.-S. Fan, Chemically and physically robust, commercially viable iron-based composite oxygen carriers sustainable over 3000 redox cycles at high temperatures for chemical looping applications, Energy Environ. Sci. 10 (11) (2017) 2318–2323.

[22] B. Fleiß, J. Fuchs, S. Penthor, S. Arlt, R. Pachler, S. Müller, H. Hofbauer, Innovative laboratory unit for pre-testing of oxygen carriers for chemical-looping combustion, Biomass Conversion and Biorefinery, https://doi.org/10.1007/s13399-021-01530-w.

[23] J. Adánez, L.F. de Diego, F. García-Labiano, P. Gayán, A. Abad, J.M. Palacios, Selection of oxygen carriers for chemical-looping combustion, Energy Fuels 18 (2) (2004) 371–377.

[24] R.A. Young, The Rietveld Method, Oxford University Press, 1995.

[25] M. Johansson, T. Mattisson, A. Lyngfelt, Investigation of Fe2O3 with MgAl2O4 for chemical-looping combustion, Ind. Eng. Chem. Res. 43 (22) (2004) 6978–6987.

[26] W. Hu, F. Donat, S.A. Scott, J.S. Dennis, The interaction between CuO and Al2O3 and the reactivity of copper aluminates below 1000 degrees C and their implication

on the use of the Cu-Al-O system for oxygen storage and production, RSC Adv. 6 (2016), 113016.

[27] L.F. de Diego, F. García-Labiano, P. Gayán, J. Celaya, J.M. Palacios, J. Adánez, Operation of a 10 kW$_{th}$ chemical-looping combustor during 200 h with a CuO–Al$_2$O$_3$ oxygen carrier, Fuel 86 (7-8) (2007) 1036–1045.

[28] A. Coppola, F. Scala, L. Gargiulo, P. Salatino, A twin-bed test reactor for characterization of calcium looping sorbents, Powder Technol. 316 (2017) 585–591.

[29] M. Pishahang, Y. Larring, R.E. Stensrød, K.A. Andreassen, A.I. Spjelkavik, 3kW circulating fluidized bed chemical looping reactor - A thermochemical and chemomechanical investigation on the performance of Cu- impregnated Al$_2$O$_3$ as an oxygen carrier material, Int. J. Greenhouse Gas Control 109 (2021), 103384.

[30] J. Adánez, C. Dueso, L.F. de Diego, F. García-Labiano, P. Gayán, A. Abad, Methane combustion in a 500 W$_{th}$ chemical-looping combustion system using an impregnated Ni-based oxygen carrier, Energy Fuels 23 (1) (2009) 130–142.

[31] P. Kolbitsch, T. Pröll, J. Bolhar-Nordenkampf, H. Hofbauer, Characterization of chemical looping pilot plant performance via experimental determination of solids conversion, Energy Fuels 23 (3) (2009) 1450–1455.

[32] L.F. de Diego, M. Ortiz, F. García-Labiano, J. Adánez, A. Abad, P. Gayán, Hydrogen production by chemical-looping reforming in a circulating fluidized bed reactor using Ni-based oxygen carriers, J. Power Sources 192 (1) (2009) 27–34.

[33] O. Condori, F. García-Labiano, L.F. de Diego, M.T. Izquierdo, A. Abad, J. Adánez, Biomass chemical looping gasification for syngas production using ilmenite as oxygen carrier in a 1.5 kW$_{th}$ unit, Chem. Eng. J. 405 (2021), 126679.

[34] S. Lamouri, M. Hamidouche, N. Bouaouadja, H. Belhouchet, V. Garnier, G. Fantozzi, J.F. Trelkat, Control of the γ -alumina to α-alumina phase transformation for an optimized alumina densification, Boletín de la Sociedad Española de Cerámica y Vidrio 56 (2017) 47–54.

[35] P. Gayán, M.A. Pans, M. Ortiz, A. Abad, L.F. de Diego, F. García-Labiano, J. Adánez, Testing of a highly reactive impregnated Fe$_2$O$_3$/Al$_2$O$_3$ oxygen carrier for a SR–CLC system in a continuous CLC unit, Fuel Process. Technol. 96 (2012) 37–47.

[36] M. Rydén, D. Jing, M. Källén, H. Leion, A. Lyngfelt, T. Mattisson, CuO-based oxygen-carrier particles for chemical-looping with oxygen uncoupling (CLOU) – experiments in batch reactor and in continuous operation, Ind. Eng. Chem. Res. 53 (2014) 6255–6267.

[37] P. Hallberg, M. Hanning, M. Rydén, T. Mattisson, A. Lyngfelt, Investigation of a calcium manganite as oxygen carrier during 99 h of operation of chemical-looping combustion in a 10 kW$_{th}$ reactor unit, Int. J. Greenhouse Gas Control 53 (2016) 222–229.

[38] D. Zeng, Y. Qiu, M. Li, L. Ma, D. Cui, S. Zhang, R. Xiao, Spatially controlled oxygen storage materials improved the syngas selectivity on chemical looping methane conversion, Appl. Catal., B. 281 (2021) 119472.

[39] Y.u. Qiu, L.i. Ma, D. Zeng, M. Li, D. Cui, Y. Lv, S. Zhang, R. Xiao, Efficient CO$_2$ to CO conversion at moderate temperatures enabled by the cobalt and copper co-doped ferrite oxygen carrier, J. Energy Chem. 46 (2020) 123–132.